FOUR-DIMENSIONAL B-SPLINE ALGORITHM FOR MARS CRATER RECONSTRUCTION

Maged Marghany and Shattri Mansor
Geospatial Information Science Research
Centre, Faculty of Engineering
University Putra Malaysia
43400 UPM, Serdang, Selangor
Email :magedupm@hotmail.com

KEY WORDS: Mars, Crater, High Resolution Stereo Camera (HRSC), Four-dimensional, B-spline.

ABSTRACT: The main contribution of this work is to simulate 4-D of Mars carters. In doing so, 3-D data of High Resolution Stereo Camera (HRSC) was aquired and then 4-D spline algorithm implemented to sequences of HRSC data with different fram of times. The study shows that B-spline can determine the 4-D crater surface with deep ice covers which could indicate for the existence of water. In conclusion, integration between 4-D B-spline algorithm and High Resolution Stereo Camera can be excellent 4-D visualization tool.

1. INTRODUCTION

A carter is most visual feature which exists in Mars surface. Crater can be created by two cosmic bodies crashed each other, for instance, a meteorite striking a planet. It can be also formed by volcanic occupation. The different sort of carter is subsidence crater, which is occurred from an underground due to nuclear explosion. A crater-like pattern shaped by erosion which is known as Machtesh. Furthermore, a relief crater triggered by a phreatic outburst or explosion is defined as a maar crater. Therefore, Mars is a terrestrial planet which contains of minerals. These minerals are containing silicon and oxygen, metals, and other elements which naturally form rock. The Mars surface is mostly created from tholeiitic basalt. With these regards, the Mars is required standard procedures to understand its complicated nature and characteristics formation. In fact, man has a great attention to explore Mars to be alternative settlement of the Earth. At present, Marghany (2015) has implemented the fourth-dimensional algorithm to study the geological carter features of the Mars. Consequently, the preliminary geologic studies of Mars derived from ground-based telescopic observations when the Mars and the Earth were neighboring and the spatial resolution was arisen up to 100 km lower than the greatest earthbound atmospheric surroundings (Martin et al*.,* 1992 and Rencz, 1999). Further, spacecraft orbiting Mars have delivered images of canyons and flood valleys features which suggest the existence of water flows on the Mars surface. Nowadays, nonetheless, Mars is a cold, dry, desert like world through a cracked atmosphere. Thus, no known organism could survive on the Red Planet in the absence of water flows (de Vaucouleurs, 1954; Mutch *et al.,* 1976).

Remote sensing technologies have attempted to explore the Mars surface. Spectroscopic remote sensing observations for instance, can provide widely investigative compositional and mineralogical information on the Mars surfaces. Basically, three categories of spectroscopic observations can be attained: (i) thermal emission spectra; (ii) reflectance spectra, and (iii) X-ray and gamma-ray spectra. Consequently, orbital visible and thermal-IR imaging and spectroscopic analyses by the Mariner 9 and Viking missions showing lavish supplementary geologically multifaceted surface which has been shaped by volcanic, tectonic, impact, and gradational processes. Credibly most discovery of dendritic valley network systems which were originated by the action of liquid water on the surface (Carr, 1996). Further, thermal-IR images and near-IR imaging spectroscopic data, conveying evidence on the surface thermos-physical properties and mineralogy for inadequate area of the Martian surface (Rencz 1999; Hartmann, 2003). Moreover, X-ray and gamma ray are proficient to precisely extricate any object from its parent galaxy, and govern physical intensity in the nucleus, arms and halo of spiral galaxy. Nonetheless, the shinning objects that extract from spiral galaxy for instance by X-rays and gamma rays can be tiny and vary on timescales of few minutes or few seconds (Evans *et al.* 1993; Yin *et al.* 1993; Burns 1993; Gaffey et al. 1993).

Christensen, (1986) and Kahle et al., (1993) conveyed that thermal emission spectra have been expended, for instance, to obtain an evidence on variations in continental basaltic lava flows and to confine rock abundance of the Martian surface and the thermal inertia. Additionally, Shelley (2008) stated that the Hubble Space Telescope (HST) is considered the NASA's great space observatories in addition to the Spitzer space Telescope, the Chandra X-ray and the Compton Gamma Ray space Observatories. These space observatories are designed to work with high spectra energy coverage which ranged from 20 keV to 30 GeV.

According to Marghany (2015), European Space Agency (ESA) has founded the MARS express mission which aimed at examining the surface, subsurface, atmosphere and ionosphere of the Mars. The devices are expended for surface and subsurface studies are implicated (i) High resolution Stereo Camera (HRSC); (ii) Visible and Infrared Mineralogical Mapping Spectrometer (OMEGA) and; Subsurface Sounding Radar Altimeter (MARSIS). Accordingly, the atmosphere and Ionosphere devices are: (i) Energetic Neutral Atoms Analyzer (ASPERA); (ii) Planetary Fourier Spectrometer (PFS) and (iii) Ultraviolet and Infrared Atmospheric Spectrometer (SPICAM). Moreover, radio link instrument which is Mars Radio Science Experiment (MaRS). Conclusively, HRSC delivers 3-D images of geological features of the Mars which contains of surface, crust, and interior of the Mars. Certainly, the term planetary geology science is to study the solid parts of moons and planets.

The novelty of this work is to design algorithm for visualization of crater features in four-dimensional using High resolution Stereo Camera (HRSC) images. In fact, HRSC can imagine object in 3-D. With this regard, the main hypotheses is that 4-D of any object in space is coded into 3-D as 3-D is coded into 2-D. On other words, n+1 D is coded into n-D. Through advanced algorithm in computer vision, 4-D spline algorithm is believed to use in n-D visualization. With this regard, the study aims at utilizing 4-D spline to generate 4-D of crater surfaces from the stereo of craters which are obtained by High resolution Stereo Camera (HRSC).

2. DATA SETS

On June 2, 2003, ESA's space probe Mars Express (Figure 1) was launched by a Soyuz-Fregat rocket from Baikonur Cosmodrome in Kazakhstan. It entered the elliptical orbit of Mars on December 25, 2003. The orbit of Mars Express has a maximum distance of 10,530 km above the Martian surface and 330 km on adjoining approach. This physical geometry grants for examinations of the Mars moons Phobos and Deimos along with measuring its atmospheric profile.

Figure 1. Mars Express in orbit around Mars.

Following Marghany (2015), the crater data are obtained from HRSC. The HRSC is mapping the Mars in 3-D with a resolution of approximately 10 metres (Figure 2). Specific areas was imaged at 2 m resolution. This is because of the camera encompasses ultra-high-resolution telephoto lens besides Super Resolution Channel (SRC), which is imaging objects two to three metres in size (DLR 2015). In initial stage, the mission of HRSC is aimed at searching liquid waters and life in the Red Planet's surface. To date, about 75% of the Martian surface has been covered in 3-D.

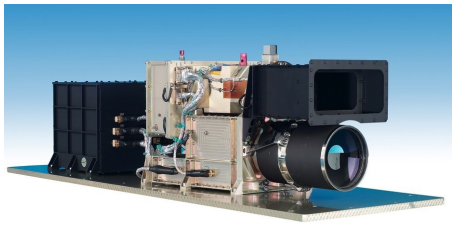

Figure 2. High Resolution Stereo Camera HRSC.

The HRSC camera system, which only weighs 20 kilograms, has two camera heads: the High Resolution Stereo head, which consists of nine CCD line sensors mounted in parallel behind a lens, and the SRC head, which is composed of a mirror telephoto lens and a CCD array sensor. In this case, each sensor records the same object on the surface at a

different angle. Three-dimensional images are generated by five of the image strips. The remaining four of the nine line sensors are equipped with special colour filters for recording multi-spectral data (Figure 3).

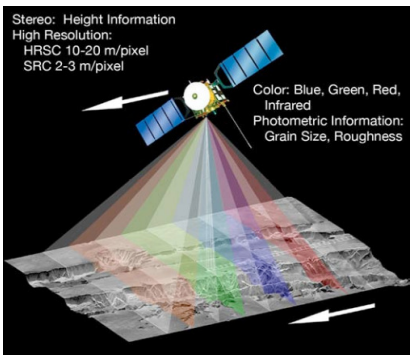

Figure 3. HRSC camera scanning system.

Approximately the shortest distance of 270 km from the spacecraft. Consequently, the resolution of the 9 image strips at this height is 12 metres for each of the 5184 seven-micron square pixels. The sensor has swath of 52 kilometres and the minimum strip length of 300 kilometres. The latter depends on the spacecraft's data storage and transmission capacity. The Super Resolution Channel (SRC) is used as a magnifying glass. At the epicentre, it delivers images of 2.3 km by 2.3 km wide in the centre of the image strips; the surface details are imaged with a resolution of 2.3 metres per pixel. The SRC recordings offer a geological background of the zone, which is delivered by the high-resolution imageries which are obtained with the stereo head (DLR 2015 and Marghany 2015).

3. FOUR-DIMENSIONAL ALGORITHM

The dimension of a mathematical space, in physics and mathematics is confidentially delineated for instance, the minimum number of coordinates required to identify any point contained by it. Space and time, in classical mechanics are diverse classes and denote to supreme space and time. That conception of the objects is a four-dimensional (4-D) space, nonetheless not the one that was originated essential to express electromagnetism. 4-D of space-time involve occasions which are not absolutely termed spatially and temporally (Amini et al., 1998a;Marghany 2003; Marghany 2011;Marghany 2015). On the other hand relatively are known as virtual to the motion of an observer. With these regards, any object can be drive in the space of four and even higher dimensions. The key challenge is to regulate rationality approaches to renovate such high-dimensional stuffs. Following Marghany (2015), 4-D spline is used to simulate 4-D of crater from sequences of HRSC images. Let u, v, and w are constrained to the interval $u, v, w \in [0, 1]$ and S $(u, v, w, t) \in (x, y, z)$ (Amini et al.,1998b). This means that the object is divided into hyperpatches. The hyperpatches are represented using surfaces and curves. Then, the surface defined by setting one of u, v, w to a constant integer value which is yelled a knot plane which are the defining the surfaces of hyperpatches (Mortenson 1985). The points in the interior and on the boundary of the parametric solid is given by (Mortenson 1985),

$$p(u,v,w) = [x\ y\ z] = [x(u,v,w) \quad y(u,v,w) \quad z(u,v,w)] \tag{1.0}$$

$$u_{\min} \le u \le u_{\max}; \tag{1.1}$$

$$v_{\min} \le v \le v_{\max}; \tag{1.2}$$

$$w_{\min} \le w \le w_{\max} \tag{1.3}$$

The 4-D B-spline curve is defined by the following equation ($n_k = n$):

$$\mathbf{C}(t) = \mathbf{N}_{1\times n} \cdot \mathbf{P}_{n\times 3} = \left(N_{0,p}(t) \quad N_{0,p}(t) \quad \ldots \quad N_{n-1,p}(t)\right) \begin{pmatrix} P_{0,x} & P_{0,y} & P_{0,z} & P_{0,t} \\ P_{1,x} & P_{1,y} & P_{1,z} & P_{1,t} \\ .. & .. & .. & .. \\ P_{n-1,x} & P_{n-1,y} & P_{n-1,z} & P_{n-1,t} \end{pmatrix}, \tag{2.0}$$

where $N_{i,p}(t)$ – the B-spline basis functions and a control point matrix is $\boldsymbol{P}_{n\times 3}$. To implement the 4-D spline, the 3D HRSC data which is acquired at individually knot time and knot planes become temporal functions. Then the detected features in 3D HRSC can be expressed in 4-D B-spline model as (Amini et al., 1998a):

$$R(u,v,w,t)=\sum_{i=1}^{I}\sum_{j=1}^{J}\sum_{k=1}^{K}\sum_{l=1}^{L}P_{ijk}O_i(u)O_j(v)O_k(w)O_l(t) \qquad (3.0)$$

where $O_i(u)$, $O_j(v)$, $O_k(w)$, and $O_l(t)$ are B-spline basis functions which blend control points $\boldsymbol{P}_{n\times 3}$ and ($I \times J \times K \times L$) is the total number of model control points. By changing the order of B-spline summation, a more efficient approach to computing a multi-dimensional B-spline model results. The simulated data included 300 frames. The fitting algorithm converged in about 30 iterations. Therefore, the total fitting process approximately took 588 seconds for 6 frames of data. An important byproduct of our approach is that at the conclusion of fitting knot solid to frames of data, a 4-D model S (u, v, w, and t) is determined. Given two solids S (u, v, w, t_0) and S (u, v, w, t_1), a 3-D B-spline interpolated motion field is immediately generated by employing the computation in (Amini et al., 1998b):

$$\mathrm{V}(u,\ v,\ w)=\mathrm{S}_1(u,\ v,\ w,\ t_1)-\mathrm{S}_0(u,\ v,\ w,\ t_0) \qquad (4.0)$$

The 4-D shape model is self-regulating of the intrinsic description of 3-D and 4-D figures when landmarks are existing. It can be easily extended to 4-D case after normalizing the number of phases per different sub-images of all frames to subjective number of data. In this study we used 30 frames, and employing the landmark creation algorithm continuously for each phase of 30 frames over time t. Then, a series of elastic transforms are implemented to convey the transmitted landmarks on top of the crater surface. The following equation is used for a series of elastic transforms as

$$\mathrm{T}_{elastic}(u,v,w,t)=[u,v,w,t]^T+\sum_{i=1}^{I}\sum_{j=1}^{J}\sum_{k=1}^{K}\sum_{l=1}^{L}P_{ijk}O_i(u)O_j(v)O_k(w)O_l(t)M_{i+l,j+m,k+n,L+o} \qquad (5.0)$$

where M denotes N_u x N_v x N_w x N_t mesh for control point of $[u,v,w,t]^T$ which are identified within a volume of dimension of $[U,V,W,t]$. The elastic transforms were achieved with a series of B-spline changes by four levels of meshes, (4×4×4), (6 × 6 × 6), (8 × 8 × 8), and (16 × 16 × 16). Its allied control points for each mesh level, M are adjusted to minimize the space between the distorted landmarks and the number of object surface.

4. RESULT AND DISCUSSIONS

The digital Elevation Model of craters within the Hellas Basin is shown in Figure 4. It is interesting to find that the DEM varies between -3 km to 6 km. Craters geographical location is 29°S, and 68°E in northern rim of Hellas basin. This data is acquired on 8 Jul. 2004 by HRSC camera. According to Marghany (2015), the Hellas Basins have formed between between 3.8 and 4.1 billion years ago, after a great asteroid hit the Mars surface. These Hellas basins were modified by the impacts of action of wind, ice, water and volcanic activity since they were formed. Further, HRSC was able to imagine the craters with the ground resolution is about 15 meters per pixel with 25 km across. Figure 5, shows the simulated crater DEM which ranged from -3km to 3km. The lowest point of DEM of -3km is located in deep of the crater.

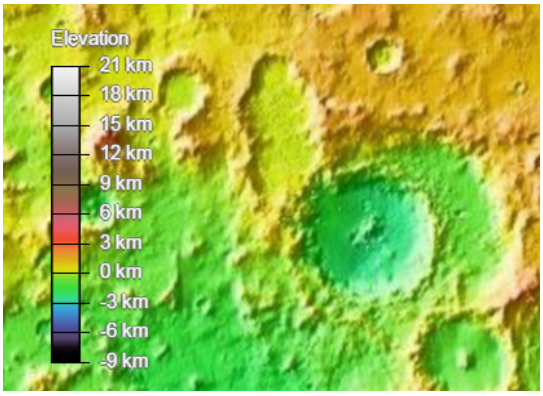

Figure 4. Craters DEM Hellas Basin.

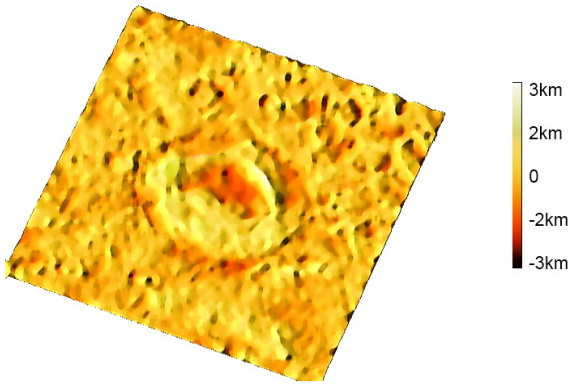

Figure 5. 3-D of crater simulated by B-spline.

The larger of the two craters is about 25 km across. Therefore, the morphology of many features in the Hellas Basin and its surroundings strongly suggests the presence of ice and glaciers. The HRSC can produced 3-D of Mars geological features because of the High Resolution Stereo head works on push broom mode: sensors image a line on the planet surface perpendicular to the ground track of the spacecraft and rely on the orbital motion of the spacecraft to reposition them as they record a sequence of images known as an image swath. This agrees with Hartmann (2003) and Carr (2006).

Figure 6 shows the 4-D of the crater which simulated using 4-D spline. It is interesting to find that 4-D layer is seen clearly as floating on the middle of crater. In addition, the deep of crater is dominated by ice which is the proof of liquid water existence. This could attribute to that within -3km in deep of crater, the atmospheric pressure is approximately 89% higher than the surrounding of the crater. This finding agrees with Marghany (2015) and ESA (2015). Truthfully, 4-D spline algorithm is separated the 3-D craters from HRSC data into hyperpatches. Subsequently, the hyperpatches are implemented using surfaces and curves. Formerly, the surface labeled by tracing one of 3-D constituents to a constant integer value which are the major of hyperpatches.

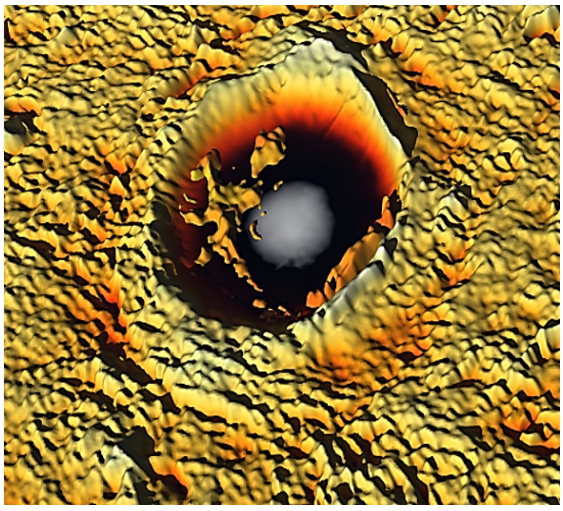

Figure 6. 4-D crater simulated by B-spline.

4-D is generated automatically by assistance of landmarks. Indeed, landmarks are automatically created and transmitted to 4D data by means of rigid alignment, distance-based merging, and B-spline transform. The energy of series of elastic transforms which are identified within a volume of 4-D dimension. This is clearly obvious in Figure 6. Additionally, the series of B-spline changes are achieved by the elastic transforms to acquire accurately 4-D of crater volumetric. The landmarks are compulsory to be consistently scattered on the crater surface and concentrated abundant subsequently that their triangular mesh is adjacent to the original crater surface. Predominantly, landmarks positioned on crater surfaces must match up to each pixel. Finally, M are adjusted to minimize the space between the distorted landmarks and the number of object surface. This study confirms the work done by Waks et al., (1996); Duda, (2001); Marghany (2014); and Marghany (2015).

5. CONCLUSIONS

This study has demonstrated a new novelty for 4-D carter surface reconstruction from HRSC data. The series of elastic transforms for B-spline are used with involving automatic detection algorithm of landmarks. The study shows that 4-D axis is seen clearly as floating objects on the middle of crater. The study also shows that the deep of crater is covered by ice which is an excellent proof of liquid water existence on the Mars. In conclusion, modification of 4-D B-spline by involving elastic transform and landmarks algorithms could be an excellent promise for 4-D visualization.

References

Amini, A.A., Y. Chen, R. W. Curwen, V. Mani, and J. Sun, 1998a, Coupled B-Snake Grids and Constrained Thin-Plate Splines for Analysis of 2-D Tissue Deformations from Tagged MRI", IEEE Transactions on Medical Imaging, 17(3):344-356.

Amini, A.A., P. Radeva, and D. Li, 1998b, Measurement of 3D motion of myocardial material points from explicit B-surface reconstruction of tagged data", Medical Image Computing and Computer-Assisted Intervention, MIT, Cambridge, MA, October 1998.

Burns R.G., 1993. Origin of Electronic Spectra of Minerals in the Visible-Near Infrared Region. In *Remote Geochemical Analysis: Elemental and Mineralogical Composition ,* ed. C.M. Pieters and P.A.J. Englert, pp. 3-29. Cambridge: Cambridge Univ. Press.

Carr, M 2006. *The surface of Mars*. Cambridge, UK: Cambridge University Press.

de Vaucouleurs G., 1954. Physics of the Planet Mars. Faber and Faber, London.

Duda, R. O. , Hart, P. E. and Stork, D. G. 2001. Pattern Classification. John Wiley & Sons, Inc.

ESA 2015, Craters within the Hellas Basin.http://www.esa.int/spaceinimages/Images/2014/08/Craters_within_the_Hellas_Basin. [Access on August 20 2015].

Christensen, P.R., 1986. The spatial distribution of rocks on Mars, *Icarus, 68,* 217-238.

Evans, L.G., R.C. Reedy, and J.I. Trombka, (1993). Introduction to planetary remote sensing gamma ray spectroscopy, in *Remote Geochemical Analysis: Elemental and Mineralogic Composition,* C.M. Pieters and P.A.J. Englert, eds., Cambridge Univ. Press, pp. 167-198.

Gaffey S.J., L.A. McFadden, and D.B. Nash, 1993. Ultraviolet, visible, and near-infrared reflectance spectroscopy: Laboratory spectra of geologic materials. In *Remote Geochemical Analysis: Elemental and Mineralogical Composition*, C.M. Pieters and P.A.J. Englert, eds., pp. 43-71. Cambridge: Cambridge Univ. Press.

Hartmann, W. (2003). *A Traveler's Guide to Mars: The Mysterious Landscapes of the Red Planet*. New York: Workman Publishing.

Kahle, A.B., F.D. Palluconi, and P.R. Christensen, 1993. Thermal emission spectroscopy: Application to the Earth and Mars, in *Remote Geochemical Analysis: Elemental and Mineralogical Composition*. C.M. Pieters and P.A.J. Englert, eds., Cambridge Univ. Press, pp. 99-120.

Marghany, M., 2003, July. Polarised AIRSAR along track interferometry for shoreline change modeling. In *Geoscience and Remote Sensing Symposium, 2003. IGARSS'03. Proceedings. 2003 IEEE International* (Vol. 2, pp. 945-947). IEEE.

Marghany, M., 2011. Modelling shoreline rate of changes using holographic interferometry. *International Journal of Physical Sciences*, *6*(34), pp.7694-7698.

Marghany M., 2014. Hologram interferometric SAR and optical data for fourth-dimensional urban slum reconstruction. Proceedings of 35 th Asian conference on remote sensing, Nay Pyi Taw, Myanmar from 27- 31, October 2014. http://a-a-r-s.org/acrs/administrator/components/com.../OS-303%20.pdf. [Access on August 20 2015].

Marghany M., 2015. 4-D geological feature reconstructions in Mars using High Resolution Stereo Camera (HRSC). CD of 36th Asian Conference on Remote Sensing (ACRS 2015), Manila, Philippines, 24-28 October 2015, http://www.a-a-r-s.org/acrs/administrator/components/com_jresearch/files/publications/TH2-5-5.pdf.

Martin, L.J., P.B. James, A. Dollfus, K. Iwasaki, and J.D. Beish, 1992. Telescopic observations: Visual, photographic, polarimetric, in *Mars* , edited by H.H. Kieffer, B.M. Jakosky, and M.S. Matthews, pp. 34-70, Univ. of Ariz. Press, Tucson.

Mortenson,M.E.1985,Geometric Modeling. John Wiely& sons,NewYork.

Mutch, T.A., R.E. Arvidson, J.W. Head III, K.L. Jones, and R.S. Saunders, 1976. *The Geology of Mars,* Princeton Univ. Press, Princeton NJ.

Radeva, P., A mini, A., Huang, J. 1997. Deformable B-solids and implicit snakes for 3D Localization and tracking of SPAMM MRI Data. Computer Vision and Image Understanding 66, 163–178.

Rencz, A. N. 1999. *Remote sensing for the earth sciences: manual of remote sensing Volume 3* (No. Ed. 3). John Wiley and sons.

Sheehan, W., 1988. *Planets and Perception,* Univ. Arizona Press.

Shelley C., (2008) NASA's Great Observatories. NASA. Retrieved April 26, 2008

Waks, E., Prince, J., Douglas, a 1996. Cardiac Motion Simulator for Tagged MRI. Mathematical Methods in Biomedical Image Analysis, 182–191.

Yin, L.I., J.I. Trombka, I. Adler, and M. Bielefeld, 1993. X-ray remote sensing techniques for geochemical analysis of planetary surfaces, in *Remote Geochemical Analysis: Elemental and Mineralogical Composition,* C.M. Pieters and P.A.J. Englert, eds., Cambridge Univ. Press, pp., 199-212.